NANO LETTERS

pubs.acs.org/NanoLett

Letter

Dislocations as Single Photon Sources in Two-Dimensional Semiconductors

Xiaocheng Zhou, Zhuhua Zhang,* and Wanlin Guo*

Cite This: *Nano Lett.* 2020, 20, 4136–4143

Read Online

ACCESS | Metrics & More | Article Recommendations | Supporting Information

ABSTRACT: Single photon sources hold great promise in quantum information technologies and are often materialized by single atoms, quantum dots, and point defects in dielectric materials. Yet, these entities are vulnerable to annealing and chemical passivation, ultimately influencing the stability of photonic devices. Here, we show that topologically stable dislocations in transition metal dichalcogenide monolayers can act as single photon sources, as supported by calculated defect levels, diploe matrix elements for transition, and excitation lifetimes with first-principles. The emission from dislocations can range from 0.48 to 1.29 eV by varying their structure, charge state, and chemical makeup in contrast to the visible range provided by previously reported sources. Since recent experiments have controllably created dislocations in monolayer materials, these results open the door to utilizing robustly stable defects for quantum computing.

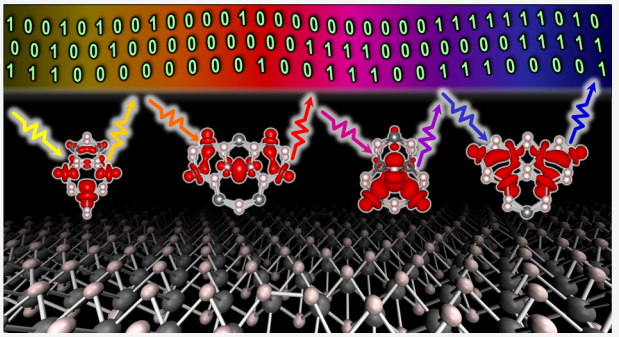

KEYWORDS: *single photon emission, dislocation, two-dimensional transition metal dichalcogenide, ab initio calculation*

Quantum information technology based on photonic qubits relies on the development of new light sources capable of creating controlled photon number. Particularly useful is the source that emits single photons at predetermined times in a solid-state platform. This source often needs a distinctive two-level quantum system, a ground state and an excited state in the same spin channel, within a dielectric material that can energetically isolate the two levels from host band edges. Then, stimulating the system can drive an optical transition between the two levels, emitting a single photon at a time. A paramagnetic entity with localized transition levels in a dielectric environment can be qualified for single photon emission (SPE), which was originally observed in resonance fluorescence of single atoms and ions,[1,2] later extended to single molecules,[3,4] quantum dots,[5,6] and atomic defects in crystals,[7−11] notably nitrogen-vacancy (NV) centers in diamond.[9] Yet, these quantum systems are subject to shortcomings, such as limited photon-extraction efficiency due to internal reflection in bulk crystals, poor control of quantum emission locations, difficult device integration, and long radiative lifetime.[9,12]

The advent of two-dimensional (2D) materials has offered new opportunities for achieving improved light-matter interaction.[13−16] Two-dimensional materials, like an open canvas, exhibit a sheer openness to enable all atoms to shower in light and allow optical transparency to facilitate the extraction of emitted photons. When defects are created in 2D space, spatial confinement and reduced dielectric screening tend to reduce their effective defect Bohr radii[17,18] and result in more localized, deeper defect levels within the bandgap, in favor of forming a two-level quantum system for SPE. Meanwhile, the radiative rate[19] and oscillator strength[20] are inversely proportional to dielectric constants and thus are larger in 2D materials than in bulk, favoring an enhanced quantum efficiency of the optical transition between the ground and excited levels in 2D semiconductors. Two-dimensional materials are also more compatible to traditional lithographic methods for device processing and integration than bulk materials with color centers are. Moreover, 2D transition metal dichalcogenides (TMDs) cover a large family of semiconductors with a wide range of bandgaps, offering great choices to explore SPE sources in a range of desired spectra.

As such, SPEs have been actively studied in a series of 2D materials, including TMDs[21−36] and hexagonal boron nitride (h-BN)[37−43] monolayers. In 2D WSe_2, quantum emissions were identified to be from edges of flakes[23,25] or atomic[22] and quantum dot-like defects[21,24] which may bind localized excitons. Nonuniform local strain was also employed to induce and tune SPEs in 2D WSe_2,[27−30,32] MoS_2,[33] $MoSe_2$,[31] and

Received: December 25, 2019
Revised: May 23, 2020
Published: May 26, 2020

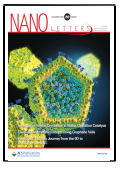

https://dx.doi.org/10.1021/acs.nanolett.9b05305
Nano Lett. 2020, 20, 4136–4143

WS_2.[28] The strain perturbation, induced by nanopillars, nanopyramids, or wrinkles, leads to a potential well in the 2D atomic lattice, which can funnel free excitons into the strain center to generate SPEs via recombination. Yet, the SPEs in TMDs often occur at cryogenic temperatures and their exact origin remains to be fully understood. Recently, a theoretical study suggested a paramagnetic impurity-vacancy center in 2D TMDs as a two-level quantum system to achieve effective emission of single photons.[44] Paramagnetic vacancies and composite defects in 2D h-BN can introduce deeper levels for optical transitions,[45,46] which enable SPEs even at room temperature,[40,41,43] as further supported by subsequent theories.[40,43,47]

Single photon sources based on vacancies, impurities, and edges in 2D semiconductors suffer from limitations in applications, as these imperfections are vulnerable to chemical passivation or thermal annealing. In contrast, dislocation, a global topological defect (with an invariant **b** called Burgers vector), is impossible to be removed by local atomic rearrangement and hence is robustly more stable.[48−51] Edge dislocations in 2D materials can separately exist along small-angle grain boundaries or be created by applying in-plane shear stress and electronic irradiation.[52−55] A number of studies have shown that dislocations can significantly modify the properties of 2D materials.[56−62] Here, we show first-principles evidence that dislocations in 2D MX_2 (M = Mo, W; X = S, Se, Te) can serve as single photon sources. By varying the charge state and chemical composition, several experimentally identified dislocations can emit single-photons in an infrared range of 0.48−1.29 eV, complementary to previously reported quantum sources limited in the visible range. In particular, the Se-rich pentagon−heptagon (5|7) dislocation and the −1 charged tetragon−hexagon (4|6) dislocations in 2D WSe_2 are predicted to emit single photons in the infrared range with minimal decoherence, suitable for applications in optical fiber telecommunication[63] and rarely achievable in other quantum systems. These results suggest a compelling interplay between photons, charges, and spin degrees of freedom in dislocations and open a new avenue for exploring quantum optics in 2D MX_2.

RESULTS AND DISCUSSION

An ideal single photon source should meet three criteria: (i) the system is paramagnetic and the defect levels are isolated from the host band edges to minimize decoherence. (ii) The optical transition gap is in a range suitable for detection and applications. (iii) The defect excitation should be polarized in an optical spectrum to achieve a polarization-selective control over the SPE. Among various 2D MX_2, the WSe_2 monolayer has a relatively large, direct bandgap of 2 eV,[64] which has attracted the most experimental attention in studying SPEs for its excellent optical quality and robust photoluminescence. We thus use the WSe_2 monolayer as a prototype and begin our discussion from the standard 5|7 dislocations, including Se-rich (with a Se—Se bond) and W-rich (with a W—W bond) cases.

The Se-rich 5|7 dislocation has a paramagnetic spin-doublet state. Its magnetization density is predominantly contributed by three W atoms in the heptagon (Figure 1a), consistent with previous predictions.[65] Thus, this dislocation emerges as a spin-polarized quantum dot in WSe_2 that is sought for the SPE. To this end, we look at its defect states near the Fermi level, E_f. The dislocation reduces the symmetry of the system from C_{3v} to C_{2v}, yielding two highly localized states near E_f that

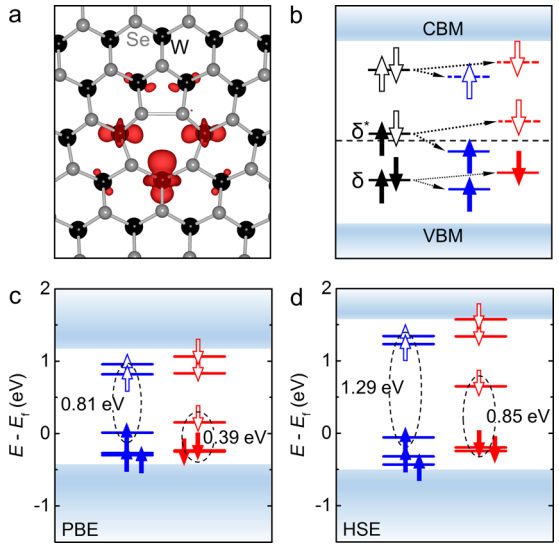

Figure 1. Two-level quantum system based on a Se-rich 5|7 dislocation in 2D WSe_2. (a) Isosurface plot (10^{-3} e/Å^3) of magnetization density of the dislocation. (b) Illustrated formation of a two-level quantum system of the dislocation. δ and δ^* denote the bonding and antibonding defect levels near the Fermi level, respectively. (c,d) Calculated defect levels with the (c) PBE and (d) HSE06 methods. The lines with solid arrows represent the filled states while those with hollow arrows are empty states. The levels in the majority and minority spin channels are colored blue and red, respectively. The shaded regions represent host bands.

dominate the spin-polarization: one marked by δ below E_f with a bonding character and the other marked by δ^* above E_f with an antibonding character (Figure 1b). The δ and δ^* states have shifted downward relative to host band states due to the lowered local potential caused by the Se—Se bond. As a result, the δ^* state almost touches the Fermi level and experiences a much larger spin-splitting than the δ state does, forming a two-level quantum system as analyzed below.

Figure 1c presents the calculated defect states within the bandgap of 2D WSe_2 for the Se-rich 5|7 dislocation using the Perdew−Burke−Ernzerhof (PBE) functional. A pair of transition levels near the Fermi level appear in each spin channel. The transition energies are 0.81 eV in the majority spin channel and 0.39 eV in the minority spin channel, also reflected in the spin-polarized density of states projected onto the Se-rich 5|7 dislocation (Figure S1a). Since calculations with the PBE functional underestimate bandgaps of 2D TMDs, we performed calculations with the hybrid Heyd−Scuseria−Ernzerhof (HSE06) functional. The results remain essentially the same, except for an increase of the transition gaps to 1.29 and 0.85 eV in the majority and minority spin channels, respectively (Figure 1d). The 1.29 eV transition suffices to prevent thermal excitation between the transition levels and enables SPE in the near-infrared region. Meanwhile, the transition levels are isolated by 0.34 eV away from the conduction band edge and 0.46 eV from the valence band edge. The isolation value is lower than 0.45 eV of a recently proposed defect complex in 2D TMDs and 0.78 eV of a defect center in h-BN,[40] but is much larger than the line width of 0.1−0.15 eV due to electron−phonon coupling associated with conduction band minimum in TMDs at room temperature.[66,67] Thus, the SPEs from the dislocation in 2D WSe_2 is expected to operate well above room temperature.

https://dx.doi.org/10.1021/acs.nanolett.9b05305
Nano Lett. 2020, 20, 4136−4143

Similar two-level system for SPE is also found for the W-rich 5|7 dislocation. The transition energy between the highest occupied and the lowest unoccupied defect levels in the majority spin channel is 1.07 eV according to HSE06 calculations (Figure S2d). However, this transition is not ideal for SPE because the highest occupied defect level is isolated only 0.02 eV away from the host valence band edge, even if the lowest unoccupied defect level is 1.09 eV away from the conduction band edge. In this sense, the Se-rich 5|7 dislocation outperforms the W-rich one in emitting single photons. It is worth mentioning that the 0.85 and 1.29 eV transitions of the Se-rich 5|7 dislocation are well separated from those of neutral (∼1.75 eV) and charged (1.72 eV) excitons in 2D WSe_2.[68] Furthermore, the excited state lifetimes of single-photons (∼1 ns)[21,22,24] are often much longer than that of excitons (<100 ps),[69] along with a line width several orders of magnitude smaller.[22] These features are helpful to experimentally identify the dislocation-induced SPEs.

The SPE from dislocations is amenable to modulation by an applied strain. For the Se-rich 5|7 dislocation, the transition energies of SPEs calculated with the PBE method in the majority and minority spin channels can be tuned by a biaxial strain at rates of 100 and 58 meV/% (110 and 67 meV/% with the HSE06 method), respectively (Figure S3), close to experimental rates ranged in 50−120 meV/%, reported on SPEs due to localized excitons in 2D WSe_2 by the strains resulting from wrinkles[29] or substrates with pillar arrays.[30]

Besides the standard 5|7 dislocations, their derivative forms, the 4|6 and 6|8 (hexagon-octagon) dislocations, have been characterized in different 2D TMDs as well.[52,70] The 4|6 dislocation can be created by removing two excess Se atoms from a Se-rich 5|7 dislocation while the 6|8 dislocation can be created by inserting two superimposed Se atoms into the W—W bond of a W-rich 5|7 dislocation. Thus, the 4|6 and 6|8 dislocations have no homoelemental bonds and exhibit a nonmagnetic ground state. Yet, the electronic properties of TMDs can be controlled by electrostatic or chemical doping. First, we consider the influence of charge doping on the defect states via an applied gate voltage (with jellium background). A −1 charged 4|6 dislocation becomes paramagnetic with a localized distribution of magnetization density (Figure 2a). The magnetism is attributed to partial filling of the δ state, which is otherwise empty in neutral charge state. This δ state undergoes a larger spin-splitting than other states do, giving rise to a spin-doublet state and qualifying the −1 charged 4|6 dislocation as a two-level quantum system.

Figure 2c presents the defect levels in the bandgap for the −1 charged 4|6 dislocation with the PBE method. A pair of transition levels appear in the majority spin channel but are absent in the minority spin channel because the highest occupied defect level is located in the host valence band. The transition energy is 0.43 eV with the PBE method and increases to 0.93 eV with the HSE06 method (Figure 2d). The transition levels are isolated by 0.92 and 0.30 eV away from the valence and conduction band edges, respectively. Therefore, the 4|6 dislocation in −1 charge state is potentially suitable for SPE in the near-infrared region.

The 6|8 dislocation in +1 charge state can also generate SPEs (Figure S4). The transition energies with the HSE06 method are 0.92 eV in the majority spin channel and 0.97 eV in the minority one. However, one of the transition levels approaches the valence band edge within 0.20 eV, which is prone to interference from the host states, unless at a cryogenic

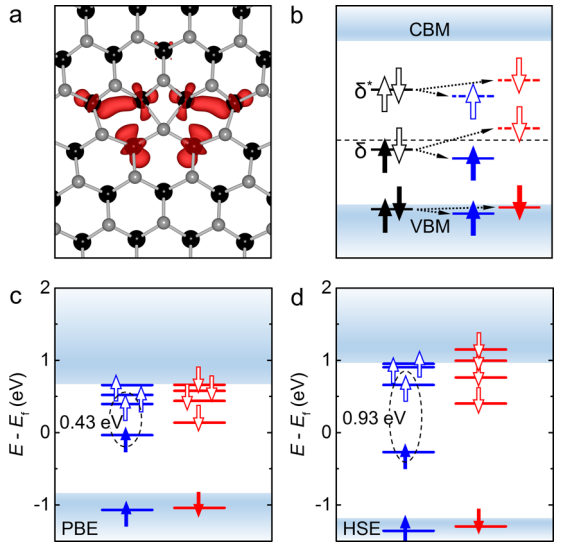

Figure 2. Two-level quantum system based on a −1 charged 4|6 dislocation in 2D WSe_2. (a) Isosurface plot (10^{-3} e/Å^3) of magnetization density of the dislocation. (b) Illustrated formation of a two-level quantum system. (c,d) Calculated defect levels with the (c) PBE and (d) HSE06 methods. Other stipulations follow the conventions described in Figure 1.

temperature, thus limiting the quantum information application of the +1 charged 6|8 dislocation.

We also study the effect of gate voltage doping on SPEs from the 5|7 dislocations. The W-rich 5|7 dislocation offers SPE in +1 charge state, while the Se-rich 5|7 dislocation does in −1 charge state (Figure S5c,d). The HSE06 results show that the transition energy is 1.10 eV in the majority spin state for the +1 charged W-rich 5|7 dislocation. Alike, the −1 charged Se-rich 5|7 dislocation offers emissions of 1.33 eV in the majority spin state and 0.80 eV in the minority spin state. Moreover, the transition levels of the −1 charged Se-rich 5|7 dislocation are isolated by at least 0.48 and 0.32 eV from the conduction and valence band edges, respectively. These results suggest that SPEs from the 5|7 dislocations can sustain across different, discrete charge states, with no apparent degradation in emission quality from their neutral cases.

In addition to charge doping, chemical substitution provides another way of regulating the SPE. Substituting Re at the W site or Br at the Se site can turn the 4|6 dislocation into the −1 charge state and make the originally nonmagnetic dislocation qualified for SPEs (Figure S6). With the HSE06 method, the transition energies are 1.08 eV for the Re_W 4|6 dislocation and 1.01 eV for the Br_{Se} one, close to 0.93 eV in the case of charge doping; the transition levels are isolated from the band edges by at least 0.30 eV. Also, the 6|8 dislocation with Ta (As) substitution at the W (Se) site offers similar transition levels to those of its +1 charged case but with more isolated transition levels from the host band states. Thus, the 4|6 and 6|8 dislocations can emit single photons via proper chemical doping as well as do the 5|7 dislocations.

To further verify the SPEs of these two-level quantum systems, we calculate the zero-phonon line emission, that is, a transition between two levels that does not involve phonons and can be detected experimentally. The PBE calculated values are 0.64 eV (majority spin) and 0.29 eV (minority spin) for the Se-rich 5|7 dislocation, 0.40 eV (majority spin) for the W-rich 5|7 dislocation, 0.47 eV (majority spin) for the −1 charged 4|6

https://dx.doi.org/10.1021/acs.nanolett.9b05305
Nano Lett. 2020, 20, 4136−4143

dislocation, as well as 0.36 eV (majority spin) and 0.48 eV (minority spin) for the +1 charged 6|8 dislocation. Most of the zero-phonon line emissions are consistent with the PBE calculated two-level transition energies.

Next, we examine whether these two-level quantum systems can be excited via illumination by computing dipole matrix elements for all possible transitions in 2D TMDs with dislocations. The imaginary part of frequency-dependent dielectric constant, Im $\varepsilon(\omega)$, is calculated to obtain the spectrum of optical absorbance. We are aware of that a dense grid of k-points and the hybrid functional should be employed for a reliable spectrum, but they are computationally demanding due to our large systems required for simulating dislocations (>200 atoms). We thus primarily employ the PBE method to seek a qualitative confirmation of SPEs, and only check the spectrum of the Se-rich 5|7 dislocation with the HSE06 method.

The Im $\varepsilon(\omega)$ spectra of the Se-rich dislocation 5|7 are shown in Figure 3a. The peaks related to defect transitions are

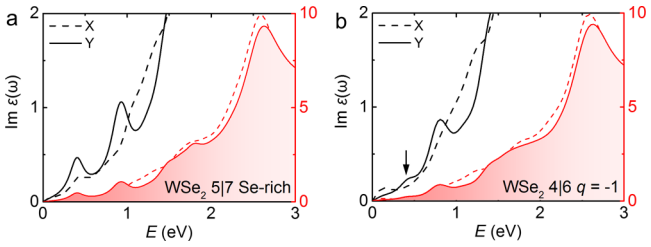

Figure 3. PBEcalculated imaginary parts Im $\varepsilon(\omega)$ of the dielectric functions for (a) the Se-rich 5|7 dislocation and (b) the −1 charged 4|6 dislocation in 2D WSe_2. The peak at ∼0.48 eV is indicated by an arrow. The spectra for the x- and y-polarized light are shown by dashed and solid lines, respectively. The black and red lines present the same results, yet with different scales as shown by the left and right ordinates.

in the energy region below 1.6 eV. The optical spectra are anisotropic due to the reduced symmetry by dislocations. The electric dipole matrix elements of the SPEs are obviously nonzero for the y-polarized light but much smaller for the x-polarized light. We thus focus our discussion on the former. Im $\varepsilon(\omega)$ of the Se-rich 5|7 dislocation shows conspicuous peaks at ∼0.40 and ∼0.90 eV, agreeing with transition energies shown in Figure 1c. Testing calculation with the HSE06 method confirms two peaks at ∼1.35 and 0.88 eV (Figure S7), respectively, again in line with the HSE06 calculated defect levels shown in Figure 1d. For the spectra of the −1 charged 4|6 dislocation shown in Figure 3b, we can identify a peak at ∼0.48 eV, tied to the level information in Figure 2c (this peak is not sharp because the used grid of k-points is not sufficiently dense). The peak at ∼0.8 eV can be ascribed to the transition associated with a higher unoccupied level. These results suggest that the SPEs from both the dislocations allow for selective excitation by the y-polarized light. We also note a small peak at ∼0.1 eV in the x-direction (Figure 3b), which does not signify SPE but is an artifact due to interaction between the 4|6 and 6|8 cores that must coexist in a supercell to apply the periodic boundary condition.

An ideal SPE should have a short excited state lifetime for a high count rate of the emission. We thus calculate the radiative lifetime, τ_r, of the SPE from dislocations in 2D WSe_2 (see details on calculations in SI-8). The shortest τ_r is ∼1 ns for the Se-rich 5|7 dislocation, which is much shorter than the excited state lifetimes (10−30 ns) of NV centers in diamond[9] due to advantages of 2D confinement in photon emission. The ∼1 ns radiative lifetime even stands out from those of color centers in recently studied 2D systems, such as WSe_2 (1−2 ns)[21,22,24] and h-BN (3 ns)[40] monolayers. This makes the dislocations in 2D TMDs promising for applications in high-speed quantum communication.

Given similar properties of the semiconducting family of 2D MX_2, the SPEs from dislocations are general to other MX_2 monolayers, including MoS_2, $MoSe_2$, $MoTe_2$, WS_2, and WTe_2. Extensive calculations prove that all semiconducting 2D MX_2 can host the dislocations as two-level quantum systems for emitting single photons, as shown in Figure 4. We collect the emission energies of early studied systems for comparison,

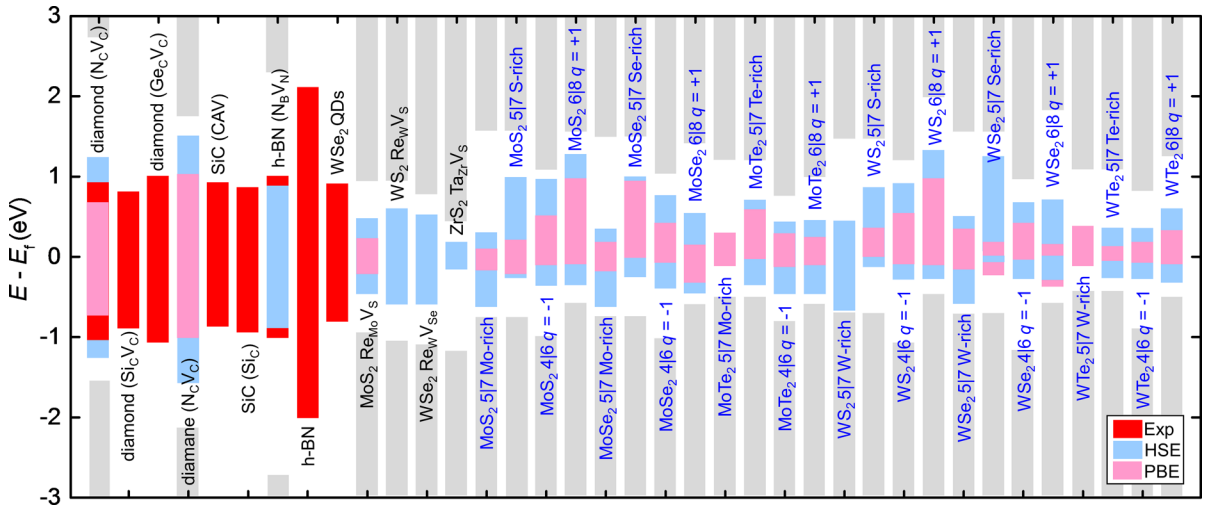

Figure 4. A summary of single photon emissions from defects in different host materials. The transition energies colored red, blue, and pink correspond to results from experiments, HSE06 and PBE calculations, respectively. The gray bars represent the conduction and valence bands of the host materials. All defects are in charge neutral state unless specified with q. The data for color centers in bulk materials and h-BN, as well as $Re_{Mo}V_S$ in MoS_2, Re_WV_S in WS_2, Re_WV_{Se} in WSe_2, and $Ta_{Zr}V_S$ in ZrS_2 are taken from references (see text). Our calculated results are indicated with blue notations.

https://dx.doi.org/10.1021/acs.nanolett.9b05305
Nano Lett. 2020, 20, 4136−4143

including experimental color centers in diamond,[7,44,71,72] SiC,[10,11] h-BN,[37,38,40] 2D WSe_2[21−24] and predicted defects in 2D materials.[44] Most of the experimentally studied systems emit in the visible range (1.68−3.06 eV). In contrast, the quantum emissions from dislocations in 2D MX_2 gather in the range of 0.48−1.29 eV, complementary to existing quantum systems and desirable for application in optical fiber telecommunication.

Compared to previous quantum systems based on point defects, the dislocations can be controllably created in 2D MX_2 using a conic substrate during synthesis,[73] as illustrated in Figure 5c. A 2D MX_2 growing on a conic substrate always

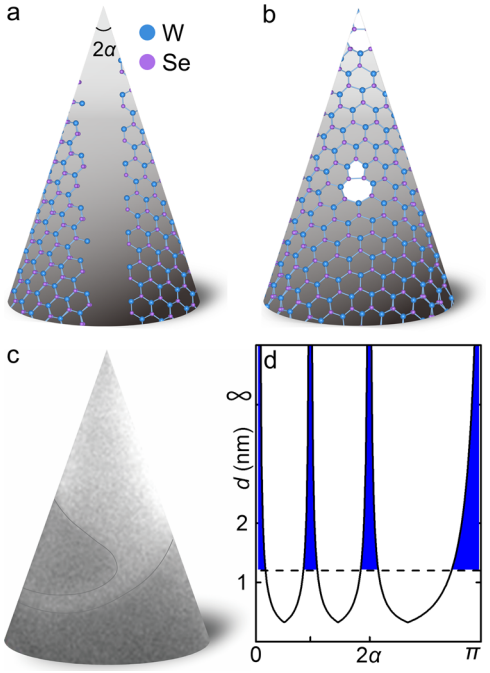

Figure 5. Controllable creation of dislocations in 2D materials. (a,b) Schematic of (a) intermediate and (b) final states of a 2D WSe_2 grown on a cone. The final state includes well-separated Se-rich 5|7 dislocations by properly selecting cone's apex angle, 2α. (c) An experimental image of a WS_2 monolayer grows on a conical substrate, adapted from ref 73. (d) Distance d as a function of 2α. Blue-shaded regions denote parameter spaces ($0 < 2\alpha < 5°$, $34° < 2\alpha < 44°$, $77° < 2\alpha < 90°$, $146° < 2\alpha < 180°$) permitting the formation of well separated dislocations in 2D WSe_2.

changes its lattice orientation and needs dislocations (or a grain boundary) to achieve a complete coverage. According to Frank equation,[74] the distance d between the dislocations along a grain boundary can be expressed as a function of its tilt angle 2θ as $d = |\mathbf{b}|/2 \sin\theta$, where $\mathbf{b}$ is the Burgers vector. Meanwhile, the tilt angle is related to the cone's apex angle 2α as $2\theta = |\mathrm{mod}(2\pi \sin\alpha + \pi/3, 2\pi/3) - \pi/3|$.[73] Thus, the relation between the distance d and cone's apex angle 2α can be written as

$$d = \frac{|\mathbf{b}|}{2\sin\left(\left|\mathrm{mod}\left(2\pi\sin\alpha + \frac{\pi}{3}, \frac{2\pi}{3}\right) - \frac{\pi}{3}\right|\right)} \quad (1)$$

When the tilt angle $2\theta < 16°$, the inter-dislocation spacing d will be at least 1.2 nm, over twice of the characteristic radius of real-space distribution of defect states and thus sufficient for electrically isolating each dislocation toward acting as a paramagnetic quantum dot. Accordingly, the apex angle of a conic substrate must be in specific ranges: $0 < 2\alpha < 5°$, $34° < 2\alpha < 44°$, $77° < 2\alpha < 90°$, $146° < 2\alpha < 180°$ (see blue regions in Figure 5d). Another point worth mentioning is that decreased chemical potential of X will favor the formation of the 4|6 and M-rich 5|7 cores over the X-rich 5|7 and 6|8 cores,[70] providing a recipe for control of dislocation structures. Further deposition of Re source onto the WSe_2 monolayer grown on the conic substrate may generate doped Re_W 4|6 dislocations via Re−W substitution at the otherwise intact dislocations, rationalized by a recent experiment showing that chemical substitution reaction preferentially occurs at dislocations in 2D MoS_2 due to strong lattice strain therein.[75]

Finally, we assess thermodynamic stability of dislocations in charge states by calculating the thermodynamic transition level. As a dislocation transitions from a q charge state to a q' state, the Fermi level shifts in response to the variation of charge state and its position where the transition occurs is the thermodynamic transition level

$$\epsilon(q/q') = \frac{1}{q' - q}\{[E_{\mathrm{tot}}(q) + qE_{\mathrm{VBM}}(q)] - [E^{\mathrm{tot}}(q') + q'E^{\mathrm{VBM}}(q')]\} \quad (2)$$

where q and q' are charges, E_{tot} is total energy of the system, and E_{VBM} is energy of the valence band maximum. We neglect the correction for the finite size effect of the supercell[76] due to the large systems considered here. The calculated thermodynamic transition levels are $\epsilon(+/0) = 0.73$ eV for the 6|8 dislocation in +1 charge state and $\epsilon(0/-) = 0.87$ eV for the 4|6 dislocation in −1 charge state in the WSe_2 monolayer (Figure S5a). These thermodynamic transition levels are within the host bandgap, such that the 0, +1, −1 charge states are all thermodynamically stable and accessible. Similar results are found for dislocations in 2D WS_2 (Figure S5b).

CONCLUSIONS

Extensive first-principles calculations have shown that dislocations in 2D transition metal dichalcogenides can exceptionally serve as single photon sources. In particular, the Se-rich 5|7 dislocation in 2D WSe_2 is an ideal two-level quantum system: its emission energy is 1.29 eV, suitable for optical fiber telecommunication, and the defect levels are isolated by at least 0.34 eV from host states, allowing for experimental excitation above room temperature. In addition, the nonmagnetic 4|6 and 6|8 dislocations can be turned into paramagnetic two-level systems by doping. The −1 charged 4|6 dislocation enables quantum emission with an energy of 0.93 eV, with the corresponding transition levels isolated by at least 0.3 eV from the host bands. Examined charge states of dislocations are thermodynamically stable and accessible by properly adjusting the Fermi energy, which further enables an electrical control on single photon emissions. Moreover, the single photons emitted by dislocations allow for polarization-selective excitations, and the estimated radiative lifetime is ∼1 ns to promise high-speed communication. The existence of a large family of 2D TMDs can further permit the fine-tuning of related parameters for single photon emissions. Since dislocations can be created controllably in any 2D materials grown on conical substrates, as demonstrated in recent experiments,[73] these results open a new avenue to studying quantum information science and technology.

https://dx.doi.org/10.1021/acs.nanolett.9b05305
Nano Lett. 2020, 20, 4136−4143

COMPUTATION METHODS

The calculations were performed with the Vienna Ab initio Simulation Package (VASP) code.[77,78] The spin-polarized density functional theory (DFT)[79,80] was based on generalized gradient approximation (GGA)[81] of the PBE functional.[82] We employed the hybrid HSE06 functional[83] for verification. The core region was described by the projector augmented wave method[84,85] with a plane-wave kinetic energy cutoff of 500 eV. A vacuum region of 12 Å was set to isolate neighboring periodic images, and a Monkhorst−Pack 5 × 5 × 1 grid of *k*-points[86] was used to sample the Brillouin Zone. The structures were fully relaxed until the force on each atom is less than 0.01 eV/Å using the PBE functional.

ASSOCIATED CONTENT

Supporting Information

The Supporting Information is available free of charge at https://pubs.acs.org/doi/10.1021/acs.nanolett.9b05305.

> Density of states of the Se-rich 5|7 and the −1 charged 6|8 dislocations, electronic properties of the W-rich 5|7 dislocation, strain effect on transition energies of the Se-rich 5|7 dislocation, electronic properties of the +1 charged 6|8 dislocation, thermodynamic transition levels and electronic properties of charged dislocations, electronic properties of chemically doped dislocations in 2D WSe_2, the HSE06 calculated imaginary parts Im $\varepsilon(\omega)$ for a Se-rich 5|7 dislocation, and details on calculations of the excited state lifetime (PDF)

AUTHOR INFORMATION

Corresponding Authors

Zhuhua Zhang − *State Key Laboratory of Mechanics and Control of Mechanical Structures, Key Laboratory for Intelligent Nano Materials and Devices of Ministry of Education, and Institute of Nanoscience, Nanjing University of Aeronautics and Astronautics, Nanjing 210016, China;* orcid.org/0000-0001-6406-0959; Email: chuwazhang@nuaa.edu.cn

Wanlin Guo − *State Key Laboratory of Mechanics and Control of Mechanical Structures, Key Laboratory for Intelligent Nano Materials and Devices of Ministry of Education, and Institute of Nanoscience, Nanjing University of Aeronautics and Astronautics, Nanjing 210016, China*; Email: wlguo@nuaa.edu.cn

Author

Xiaocheng Zhou − *State Key Laboratory of Mechanics and Control of Mechanical Structures, Key Laboratory for Intelligent Nano Materials and Devices of Ministry of Education, and Institute of Nanoscience, Nanjing University of Aeronautics and Astronautics, Nanjing 210016, China*

Complete contact information is available at: https://pubs.acs.org/10.1021/acs.nanolett.9b05305

Author Contributions

Z.Z. conceived the project. All authors contributed to the analysis of the data.

Notes

The authors declare no competing financial interest.

ACKNOWLEDGMENTS

This work was supported by the National Key Research and Development Program of China (2019YFA0705400), National Natural Science Foundation of China (11772153, 51535005), the Natural Science Foundation of Jiangsu Province (BK20190018), the Research Fund of State Key Laboratory of Mechanics and Control of Mechanical Structures (MCMS-I-0418K01, MCMS-I-0419K01), the Fundamental Research Funds for Central Universities (NE2018002, NP2019301, NJ2019002, NJ2020003) and a Project Funded by the Priority Academic Program Development of Jiangsu Higher Education Institutions. Z.Z. would like to appreciate Prof. Yakobson in Rice U and Prof. Jihui Yang in Fudan U for their valuable discussion.

REFERENCES

(1) Kimble, H. J.; Dagenais, M.; Mandel, L. Photon antibunching in resonance fluorescence. *Phys. Rev. Lett.* **1977**, *39* (11), 691.

(2) Diedrich, F.; Walther, H. Nonclassical radiation of a single stored ion. *Phys. Rev. Lett.* **1987**, *58* (3), 203.

(3) Moerner, W. E.; Kador, L. Optical detection and spectroscopy of single molecules in a solid. *Phys. Rev. Lett.* **1989**, *62* (21), 2535.

(4) Orrit, M.; Bernard, J. Single pentacene molecules detected by fluorescence excitation in a p-terphenyl crystal. *Phys. Rev. Lett.* **1990**, *65* (21), 2716.

(5) Michler, P.; Imamoğlu, A.; Mason, M.; Carson, P.; Strouse, G.; Buratto, S. Quantum correlation among photons from a single quantum dot at room temperature. *Nature* **2000**, *406* (6799), 968.

(6) Michler, P.; Kiraz, A.; Becher, C.; Schoenfeld, W.; Petroff, P.; Zhang, L.; Hu, E.; Imamoglu, A. A quantum dot single-photon turnstile device. *Science* **2000**, *290* (5500), 2282−2285.

(7) Gruber, A.; Dräbenstedt, A.; Tietz, C.; Fleury, L.; Wrachtrup, J.; Von Borczyskowski, C. Scanning confocal optical microscopy and magnetic resonance on single defect centers. *Science* **1997**, *276* (5321), 2012−2014.

(8) Kurtsiefer, C.; Mayer, S.; Zarda, P.; Weinfurter, H. Stable solid-state source of single photons. *Phys. Rev. Lett.* **2000**, *85* (2), 290.

(9) Goss, J.; Jones, R.; Breuer, S.; Briddon, P.; Öberg, S. The twelve-line 1.682 eV luminescence center in diamond and the vacancy-silicon complex. *Phys. Rev. Lett.* **1996**, *77* (14), 3041.

(10) Yang, L.-M.; Bačić, V.; Popov, I. A.; Boldyrev, A. I.; Heine, T.; Frauenheim, T.; Ganz, E. Two-dimensional Cu_2Si monolayer with planar hexacoordinate copper and silicon bonding. *J. Am. Chem. Soc.* **2015**, *137* (7), 2757−2762.

(11) Kok, P.; Munro, W. J.; Nemoto, K.; Ralph, T. C.; Dowling, J. P.; Milburn, G. J. Linear optical quantum computing with photonic qubits. *Rev. Mod. Phys.* **2007**, *79* (1), 135.

(12) Falk, A. L.; Klimov, P. V.; Buckley, B. B.; Ivády, V.; Abrikosov, I. A.; Calusine, G.; Koehl, W. F.; Gali, Á.; Awschalom, D. D. Electrically and mechanically tunable electron spins in silicon carbide color centers. *Phys. Rev. Lett.* **2014**, *112* (18), 187601.

(13) Yin, Z.; Li, H.; Li, H.; Jiang, L.; Shi, Y.; Sun, Y.; Lu, G.; Zhang, Q.; Chen, X.; Zhang, H. Single-layer MoS_2 phototransistors. *ACS Nano* **2012**, *6* (1), 74−80.

(14) Wang, Q. H.; Kalantar-Zadeh, K.; Kis, A.; Coleman, J. N.; Strano, M. S. Electronics and optoelectronics of two-dimensional transition metal dichalcogenides. *Nat. Nanotechnol.* **2012**, *7* (11), 699.

(15) Lopez-Sanchez, O.; Lembke, D.; Kayci, M.; Radenovic, A.; Kis, A. Ultrasensitive photodetectors based on monolayer MoS_2. *Nat. Nanotechnol.* **2013**, *8* (7), 497.

(16) Baugher, B. W.; Churchill, H. O.; Yang, Y.; Jarillo-Herrero, P. Optoelectronic devices based on electrically tunable p-n diodes in a monolayer dichalcogenide. *Nat. Nanotechnol.* **2014**, *9* (4), 262.

(17) Kaindl, R. A.; Hägele, D.; Carnahan, M.; Chemla, D. Transient terahertz spectroscopy of excitons and unbound carriers in quasi-two-dimensional electron-hole gases. *Phys. Rev. B: Condens. Matter Mater. Phys.* **2009**, *79* (4), 045320.

(18) Olsen, T.; Latini, S.; Rasmussen, F.; Thygesen, K. S. Simple screened hydrogen model of excitons in two-dimensional materials. *Phys. Rev. Lett.* **2016**, *116* (5), 056401.
(19) Robert, C.; Lagarde, D.; Cadiz, F.; Wang, G.; Lassagne, B.; Amand, T.; Balocchi, A.; Renucci, P.; Tongay, S.; Urbaszek, B.; Marie, X. Exciton radiative lifetime in transition metal dichalcogenide monolayers. *Phys. Rev. B: Condens. Matter Mater. Phys.* **2016**, *93* (20), 205423.
(20) Takagahara, T. Biexciton states in semiconductor quantum dots and their nonlinear optical properties. *Phys. Rev. B: Condens. Matter Mater. Phys.* **1989**, *39* (14), 10206.
(21) Chakraborty, C.; Kinnischtzke, L.; Goodfellow, K. M.; Beams, R.; Vamivakas, A. N. Voltage-controlled quantum light from an atomically thin semiconductor. *Nat. Nanotechnol.* **2015**, *10* (6), 507.
(22) He, Y.-M.; Clark, G.; Schaibley, J. R.; He, Y.; Chen, M.-C.; Wei, Y.-J.; Ding, X.; Zhang, Q.; Yao, W.; Xu, X.; Lu, C.-Y.; Pan, J.-W. Single quantum emitters in monolayer semiconductors. *Nat. Nanotechnol.* **2015**, *10* (6), 497.
(23) Koperski, M.; Nogajewski, K.; Arora, A.; Cherkez, V.; Mallet, P.; Veuillen, J.-Y.; Marcus, J.; Kossacki, P.; Potemski, M. Single photon emitters in exfoliated WSe_2 structures. *Nat. Nanotechnol.* **2015**, *10* (6), 503.
(24) Srivastava, A.; Sidler, M.; Allain, A. V.; Lembke, D. S.; Kis, A.; Imamoğlu, A. Optically active quantum dots in monolayer WSe_2. *Nat. Nanotechnol.* **2015**, *10* (6), 491.
(25) Tonndorf, P.; Schmidt, R.; Schneider, R.; Kern, J.; Buscema, M.; Steele, G. A.; Castellanos-Gomez, A.; van der Zant, H. S.; de Vasconcellos, S. M.; Bratschitsch, R. Single-photon emission from localized excitons in an atomically thin semiconductor. *Optica* **2015**, *2* (4), 347−352.
(26) Clark, G.; Schaibley, J. R.; Ross, J.; Taniguchi, T.; Watanabe, K.; Hendrickson, J. R.; Mou, S.; Yao, W.; Xu, X. Single defect light-emitting diode in a van der Waals heterostructure. *Nano Lett.* **2016**, *16* (6), 3944−3948.
(27) Branny, A.; Kumar, S.; Proux, R.; Gerardot, B. D. Deterministic strain-induced arrays of quantum emitters in a two-dimensional semiconductor. *Nat. Commun.* **2017**, *8*, 15053.
(28) Palacios-Berraquero, C.; Kara, D. M.; Montblanch, A. R.-P.; Barbone, M.; Latawiec, P.; Yoon, D.; Ott, A. K.; Loncar, M.; Ferrari, A. C.; Atatüre, M. Large-scale quantum-emitter arrays in atomically thin semiconductors. *Nat. Commun.* **2017**, *8*, 15093.
(29) Iff, O.; Tedeschi, D.; Martin-Sanchez, J.; Moczała-Dusanowska, M.; Tongay, S.; Yumigeta, K.; Taboada-Gutierrez, J.; Savaresi, M.; Rastelli, A.; Alonso-Gonzalez, P.; Hofling, S.; Trotta, R.; Schneider, C. Strain-tunable Single Photon Sources in WSe_2 Monolayers. *Nano Lett.* **2019**, *19* (10), 6931−6936.
(30) Kim, H.; Moon, J. S.; Noh, G.; Lee, J.; Kim, J.-H. Position and frequency control of strain-induced quantum emitters in WSe_2 monolayers. *Nano Lett.* **2019**, *19* (10), 7534−7539.
(31) Branny, A.; Wang, G.; Kumar, S.; Robert, C.; Lassagne, B.; Marie, X.; Gerardot, B. D.; Urbaszek, B. Discrete quantum dot like emitters in monolayer $MoSe_2$: Spatial mapping, magneto-optics, and charge tuning. *Appl. Phys. Lett.* **2016**, *108* (14), 142101.
(32) Luo, Y.; Shepard, G. D.; Ardelean, J. V.; Rhodes, D. A.; Kim, B.; Barmak, K.; Hone, J. C.; Strauf, S. Deterministic coupling of site-controlled quantum emitters in monolayer WSe_2 to plasmonic nanocavities. *Nat. Nanotechnol.* **2018**, *13* (12), 1137.
(33) Carmesin, C.; Lorke, M.; Florian, M.; Erben, D.; Schulz, A.; Wehling, T. O.; Jahnke, F. Quantum-dot-like states in molybdenum disulfide nanostructures due to the interplay of local surface wrinkling, strain, and dielectric confinement. *Nano Lett.* **2019**, *19* (5), 3182−3186.
(34) Linhart, L.; Paur, M.; Smejkal, V.; Burgdörfer, J.; Mueller, T.; Libisch, F. Localized inter-valley defect excitons as single-photon emitters in WSe_2. *Phys. Rev. Lett.* **2019**, *123* (14), 146401.
(35) Zheng, Y. J.; Chen, Y.; Huang, Y. L.; Gogoi, P. K.; Li, M.-Y.; Li, L.-J.; Trevisanutto, P. E.; Wang, Q.; Pennycook, S. J.; Wee, A. T. S.; Quek, S. Y. Point Defects and Localized Excitons in 2D WSe_2. *ACS Nano* **2019**, *13* (5), 6050−6059.
(36) Ziegler, J.; Klaiss, R.; Blaikie, A.; Miller, D.; Horowitz, V. R.; Alemán, B. J. Deterministic Quantum Emitter Formation in Hexagonal Boron Nitride via Controlled Edge Creation. *Nano Lett.* **2019**, *19* (3), 2121−2127.
(37) Bourrellier, R.; Meuret, S.; Tararan, A.; Stéphan, O.; Kociak, M.; Tizei, L. H.; Zobelli, A. Bright UV single photon emission at point defects in h-BN. *Nano Lett.* **2016**, *16* (7), 4317−4321.
(38) Chejanovsky, N.; Rezai, M.; Paolucci, F.; Kim, Y.; Rendler, T.; Rouabeh, W.; Favaro de Oliveira, F.; Herlinger, P.; Denisenko, A.; Yang, S.; Gerhardt, I.; Finkler, A.; Smet, J. H.; Wrachtrup, J. Structural attributes and photodynamics of visible spectrum quantum emitters in hexagonal boron nitride. *Nano Lett.* **2016**, *16* (11), 7037−7045.
(39) Shotan, Z.; Jayakumar, H.; Considine, C. R.; Mackoit, M.; Fedder, H.; Wrachtrup, J. r.; Alkauskas, A.; Doherty, M. W.; Menon, V. M.; Meriles, C. A. Photoinduced modification of single-photon emitters in hexagonal boron nitride. *ACS Photonics* **2016**, *3* (12), 2490−2496.
(40) Tran, T. T.; Bray, K.; Ford, M. J.; Toth, M.; Aharonovich, I. Quantum emission from hexagonal boron nitride monolayers. *Nat. Nanotechnol.* **2016**, *11* (1), 37.
(41) Tran, T. T.; Elbadawi, C.; Totonjian, D.; Lobo, C. J.; Grosso, G.; Moon, H.; Englund, D. R.; Ford, M. J.; Aharonovich, I.; Toth, M. Robust multicolor single photon emission from point defects in hexagonal boron nitride. *ACS Nano* **2016**, *10* (8), 7331−7338.
(42) Grosso, G.; Moon, H.; Lienhard, B.; Ali, S.; Efetov, D. K.; Furchi, M. M.; Jarillo-Herrero, P.; Ford, M. J.; Aharonovich, I.; Englund, D. Tunable and high-purity room temperature single-photon emission from atomic defects in hexagonal boron nitride. *Nat. Commun.* **2017**, *8* (1), 705.
(43) Li, X.; Shepard, G. D.; Cupo, A.; Camporeale, N.; Shayan, K.; Luo, Y.; Meunier, V.; Strauf, S. Nonmagnetic quantum emitters in boron nitride with ultranarrow and sideband-free emission spectra. *ACS Nano* **2017**, *11* (7), 6652−6660.
(44) Gupta, S.; Yang, J.-H.; Yakobson, B. I. Two-Level Quantum Systems in Two-Dimensional Materials for Single Photon Emission. *Nano Lett.* **2019**, *19* (1), 408−414.
(45) Attaccalite, C.; Bockstedte, M.; Marini, A.; Rubio, A.; Wirtz, L. Coupling of excitons and defect states in boron-nitride nanostructures. *Phys. Rev. B: Condens. Matter Mater. Phys.* **2011**, *83* (14), 144115.
(46) Huang, B.; Lee, H. Defect and impurity properties of hexagonal boron nitride: A first-principles calculation. *Phys. Rev. B: Condens. Matter Mater. Phys.* **2012**, *86* (24), 245406.
(47) Abdi, M.; Chou, J.-P.; Gali, A.; Plenio, M. B. Color centers in hexagonal boron nitride monolayers: A group theory and *ab initio* analysis. *ACS Photonics* **2018**, *5* (5), 1967−1976.
(48) Jeong, B. W.; Ihm, J.; Lee, G.-D. Stability of dislocation defect with two pentagon-heptagon pairs in graphene. *Phys. Rev. B: Condens. Matter Mater. Phys.* **2008**, *78* (16), 165403.
(49) Hashimoto, A.; Suenaga, K.; Gloter, A.; Urita, K.; Iijima, S. Direct evidence for atomic defects in graphene layers. *Nature* **2004**, *430* (7002), 870−873.
(50) Nelson, D. R. *Defects and geometry in condensed matter physics*, 1st ed.; Cambridge University Press: Cambridge, U.K., 2002.
(51) Warner, J. H.; Margine, E. R.; Mukai, M.; Robertson, A. W.; Giustino, F.; Kirkland, A. I. Dislocation-driven deformations in graphene. *Science* **2012**, *337* (6091), 209−212.
(52) Azizi, A.; Zou, X.; Ercius, P.; Zhang, Z.; Elías, A. L.; Perea-López, N.; Stone, G.; Terrones, M.; Yakobson, B. I.; Alem, N. Dislocation motion and grain boundary migration in two-dimensional tungsten disulphide. *Nat. Commun.* **2014**, *5*, 4867.
(53) Komsa, H.-P.; Kurasch, S.; Lehtinen, O.; Kaiser, U.; Krasheninnikov, A. V. From point to extended defects in two-dimensional MoS_2: Evolution of atomic structure under electron irradiation. *Phys. Rev. B: Condens. Matter Mater. Phys.* **2013**, *88* (3), 035301.
(54) Enyashin, A. N.; Bar-Sadan, M.; Houben, L.; Seifert, G. Line Defects in Molybdenum Disulfide Layers. *J. Phys. Chem. C* **2013**, *117* (20), 10842−10848.

https://dx.doi.org/10.1021/acs.nanolett.9b05305
Nano Lett. 2020, 20, 4136−4143

(55) Zhou, W.; Zou, X.; Najmaei, S.; Liu, Z.; Shi, Y.; Kong, J.; Lou, J.; Ajayan, P. M.; Yakobson, B. I.; Idrobo, J.-C. Intrinsic structural defects in monolayer molybdenum disulfide. *Nano Lett.* **2013**, *13* (6), 2615−2622.
(56) Yazyev, O. V.; Chen, Y. P. Polycrystalline graphene and other two-dimensional materials. *Nat. Nanotechnol.* **2014**, *9* (10), 755.
(57) Zhang, Z.; Yang, Y.; Xu, F.; Wang, L.; Yakobson, B. I. Unraveling the sinuous grain boundaries in graphene. *Adv. Funct. Mater.* **2015**, *25* (3), 367−373.
(58) Wei, Y.; Wu, J.; Yin, H.; Shi, X.; Yang, R.; Dresselhaus, M. The nature of strength enhancement and weakening by pentagon-heptagon defects in graphene. *Nat. Mater.* **2012**, *11* (9), 759−763.
(59) Yazyev, O. V.; Louie, S. G. Electronic transport in polycrystalline graphene. *Nat. Mater.* **2010**, *9* (10), 806−809.
(60) Fei, Z.; Rodin, A. S.; Gannett, W.; Dai, S.; Regan, W.; Wagner, M.; Liu, M. K.; McLeod, A. S.; Dominguez, G.; Thiemens, M.; Castro Neto, A. H.; Keilmann, F.; Zettl, A.; Hillenbrand, R.; Fogler, M. M.; Basov, D. N. Electronic and plasmonic phenomena at graphene grain boundaries. *Nat. Nanotechnol.* **2013**, *8* (11), 821−825.
(61) Tsen, A. W.; Brown, L.; Levendorf, M. P.; Ghahari, F.; Huang, P. Y.; Havener, R. W.; Ruiz-Vargas, C. S.; Muller, D. A.; Kim, P.; Park, J. Tailoring electrical transport across grain boundaries in polycrystalline graphene. *Science* **2012**, *336* (6085), 1143−1146.
(62) Grantab, R.; Shenoy, V. B.; Ruoff, R. S. Anomalous strength characteristics of tilt grain boundaries in graphene. *Science* **2010**, *330* (6006), 946−948.
(63) Sargent, H. E. Infrared quantum dots. *Adv. Mater.* **2005**, *17* (5), 515−522.
(64) He, K.; Kumar, N.; Zhao, L.; Wang, Z.; Mak, K. F.; Zhao, H.; Shan, J. Tightly Bound Excitons in Monolayer WSe_2. *Phys. Rev. Lett.* **2014**, *113* (2), 026803.
(65) Zhang, Z.; Zou, X.; Crespi, V. H.; Yakobson, B. I. Intrinsic magnetism of grain boundaries in two-dimensional metal dichalcogenides. *ACS Nano* **2013**, *7* (12), 10475−10481.
(66) Molina-Sánchez, A.; Palummo, M.; Marini, A.; Wirtz, L. Temperature-dependent excitonic effects in the optical properties of single-layer MoS_2. *Phys. Rev. B: Condens. Matter Mater. Phys.* **2016**, *93* (15), 155435.
(67) Hinsche, N. F.; Ngankeu, A. S.; Guilloy, K.; Mahatha, S. K.; Grubisic Cabo, A.; Bianchi, M.; Dendzik, M.; Sanders, C. E.; Miwa, J. A.; Bana, H.; Travaglia, E.; Lacovig, P.; Bignardi, L.; Larciprete, R.; Baraldi, A.; Lizzit, S.; Thygesen, K. S.; Hofmann, P. Spin-dependent electron-phonon coupling in the valence band of single-layer WS_2. *Phys. Rev. B: Condens. Matter Mater. Phys.* **2017**, *96* (12), 121402.
(68) Jones, A. M.; Yu, H.; Ghimire, N. J.; Wu, S.; Aivazian, G.; Ross, J. S.; Zhao, B.; Yan, J.; Mandrus, D. G.; Xiao, D.; Yao, W.; Xu, X. Optical generation of excitonic valley coherence in monolayer WSe_2. *Nat. Nanotechnol.* **2013**, *8* (9), 634.
(69) Wang, G.; Bouet, L.; Lagarde, D.; Vidal, M.; Balocchi, A.; Amand, T.; Marie, X.; Urbaszek, B. Valley dynamics probed through charged and neutral exciton emission in monolayer WSe_2. *Phys. Rev. B: Condens. Matter Mater. Phys.* **2014**, *90* (7), 075413.
(70) Zou, X.; Liu, Y.; Yakobson, B. I. Predicting dislocations and grain boundaries in two-dimensional metal-disulfides from the first principles. *Nano Lett.* **2013**, *13* (1), 253−258.
(71) Wang, C.; Kurtsiefer, C.; Weinfurter, H.; Burchard, B. Single photon emission from SiV centres in diamond produced by ion implantation. *J. Phys. B: At., Mol. Opt. Phys.* **2006**, *39* (1), 37.
(72) Iwasaki, T.; Ishibashi, F.; Miyamoto, Y.; Doi, Y.; Kobayashi, S.; Miyazaki, T.; Tahara, K.; Jahnke, K. D.; Rogers, L. J.; Naydenov, B.; Jelezko, F.; Yamasaki, S.; Nagamachi, S.; Inubushi, T.; Mizuochi, N.; Hatano, M. Germanium-vacancy single color centers in diamond. *Sci. Rep.* **2015**, *5*, 12882.
(73) Yu, H.; Gupta, N.; Hu, Z.; Wang, K.; Srijanto, B. R.; Xiao, K.; Geohegan, D. B.; Yakobson, B. I. Tilt grain boundary topology induced by substrate topography. *ACS Nano* **2017**, *11* (9), 8612−8618.
(74) Anderson, P. M.; Hirth, J. P.; Lothe, J. *Theory of dislocations*. 3rd ed.; Cambridge University Press: Cambridge, U.K., 2017.
(75) Zhu, C.; Yu, M.; Zhou, J.; He, Y.; Zeng, Q.; Deng, Y.; Guo, S.; Xu, M.; Shi, J.; Zhou, W.; Sun, L.; Wang, L.; Hu, Z.; Zhang, Z.; Guo, W.; Liu, Z. Strain-driven growth of ultra-long two-dimensional nanochannels. *Nat. Commun.* **2020**, *11* (1), 1−10.
(76) Freysoldt, C.; Neugebauer, J.; Van de Walle, C. G. Fully *ab initio* finite-size corrections for charged-defect supercell calculations. *Phys. Rev. Lett.* **2009**, *102* (1), 016402.
(77) Kresse, G.; Hafner, J. *Ab initio* molecular dynamics for liquid metals. *Phys. Rev. B: Condens. Matter Mater. Phys.* **1993**, *47* (1), 558.
(78) Kresse, G.; Furthmüller, J. Efficiency of *ab-initio* total energy calculations for metals and semiconductors using a plane-wave basis set. *Comput. Mater. Sci.* **1996**, *6* (1), 15−50.
(79) Hohenberg, P.; Kohn, W. Inhomogeneous electron gas. *Phys. Rev.* **1964**, *136* (3B), B864.
(80) Kohn, W.; Sham, L. J. Self-consistent equations including exchange and correlation effects. *Phys. Rev.* **1965**, *140* (4A), A1133.
(81) Langreth, D. C.; Perdew, J. P. Theory of nonuniform electronic systems. I. Analysis of the gradient approximation and a generalization that works. *Phys. Rev. B: Condens. Matter Mater. Phys.* **1980**, *21* (12), 5469−5493.
(82) Perdew, J. P.; Burke, K.; Ernzerhof, M. Generalized Gradient Approximation Made Simple. *Phys. Rev. Lett.* **1996**, *77* (18), 3865−3868.
(83) Heyd, J.; Scuseria, G. E.; Ernzerhof, M. Hybrid functionals based on a screened Coulomb potential. *J. Chem. Phys.* **2003**, *118* (18), 8207−8215.
(84) Blöchl, P. E. Projector augmented-wave method. *Phys. Rev. B: Condens. Matter Mater. Phys.* **1994**, *50* (24), 17953.
(85) Kresse, G.; Joubert, D. From ultrasoft pseudopotentials to the projector augmented-wave method. *Phys. Rev. B: Condens. Matter Mater. Phys.* **1999**, *59* (3), 1758−1775.
(86) Monkhorst, H. J.; Pack, J. D. Special points for Brillouin-zone integrations. *Phys. Rev. B: Condens. Matter Mater. Phys.* **1976**, *13* (12), 5188.

https://dx.doi.org/10.1021/acs.nanolett.9b05305
Nano Lett. 2020, 20, 4136−4143